Nuclear Engineering and Technology 55 (2023) 3301–3312

Contents lists available at ScienceDirect

Nuclear Engineering and Technology

journal homepage: www.elsevier.com/locate/net

Original Article

High fidelity transient solver in STREAM based on multigroup coarse-mesh finite difference method

Anisur Rahman [a], Hyun Chul Lee [b, *], Deokjung Lee [a, c, **]

[a] Department of Nuclear Engineering, Ulsan National Institute of Science and Technology, 50 UNIST-gil, Ulsan, 44919, Republic of Korea
[b] School of Mechanical Engineering, Pusan National University, Busan, 46241, Republic of Korea
[c] Advanced Nuclear Technology and Services, 406-21 Jonga-ro, Jung-gu, Ulsan, 44429, Republic of Korea

ARTICLE INFO

Article history:
Received 29 September 2022
Received in revised form
3 April 2023
Accepted 14 May 2023
Available online 21 May 2023

Keywords:
Transient analysis
CMFD
Rod decusping
Time step control

abstract

This study incorporates a high-fidelity transient analysis solver based on multigroup CMFD in the MOC code STREAM. Transport modeling with heterogeneous geometries of the reactor core increases computational cost in terms of memory and time, whereas the multigroup CMFD reduces the computational cost. The reactor condition does not change at every time step, which is a vital point for the utilization of CMFD. CMFD correction factors are updated from the transport solution whenever the reactor core condition changes, and the simulation continues until the end. The transport solution is adjusted once CMFD achieves the solution. The flux-weighted method is used for rod decusping to update the partially inserted control rod cell material, which maintains the solution's stability. A smaller time-step size is needed to obtain an accurate solution, which increases the computational cost. The adaptive step-size control algorithm is robust for controlling the time step size. This algorithm is based on local errors and has the potential capability to accept or reject the solution. Several numerical problems are selected to analyze the performance and numerical accuracy of parallel computing, rod decusping, and adaptive time step control. Lastly, a typical pressurized LWR was chosen to study the rod-ejection accident.

1. Introduction

Time-dependent neutron transport and multigroup diffusion equations are utilized in conventional reactor core analyses. Of the two, the transport solution is costly in terms of time and memory. In the early years, the whole-core reactor analysis with pin-wise heterogeneous geometries was not viable due to the inadequate ability of the computer. However, direct pin-wise heterogeneous whole-core calculations are becoming achievable because modern computing power is growing. Moreover, 3D pin-resolved solution in a practical reactor core is not entirely possible due to the enormous computational burden in terms of time and memory requirements [1,2]. The coarse-mesh finite difference (CMFD) method [3] is an efficient tool to reduce computing time during pin-by-pin whole-core calculation and is applied to accelerate the transport solution.

Adapting parallel hardware architecture [4] enhances computing capability, although CPU's clock speed is limited. Hence, whole-core calculations with parallel computation would be more efficient than those with a single CPU. The whole-core problem can be divided into many local problems, independent of each other, in parallel computation. Moreover, parallel processing with local problems reduces computational time and memory requirements. Finally, merging local solutions deliver a global solution.

In recent years, the neutronics code developer groups such as Variant-K [5], DeCART [6], nTRACER [7], MPACT [8], NECP-X [9], and PROTEUS-MOC [10] have paid attention to solve the 3D time-dependent neutron transport equation. The variational nodal method is used in Variant-K [5], and a homogenized cell or assembly cross-sections (XS) are required for calculation. The 2D/1D fusion method [11] is commonly used in high-fidelity transport calculation. In 2D/1D, 2D analysis is conducted by the method of characteristics (MOC), which explicitly models heterogeneous geometry in the radial direction. The 1D solution uses diffusion or SP_3 approximation with homogenized cell-level cross-sections.

* Corresponding author
** Corresponding author. Department of Nuclear Engineering, Ulsan National Institute of Science and Technology, 50 UNIST-gil, Ulsan, 44919, Republic of Korea
E-mail addresses: hyunchul.lee@pusan.ac.kr (H.C. Lee), deokjung@unist.ac.kr (D. Lee).

https://doi.org/10.1016/j.net.2023.05.019

Therefore, 2D/1D transport calculation is limited by diffusion or SP_3 approximation. The theta method discretizes the time domain with coarse mesh finite difference in DeCART [6]. At the same time, temporal time discretization with backward differentiation formula, Crank Nicolson (CN) method, and CN method with exponential transformation are available in nTRACER [7]. MPACT [8] uses a multi-level predictor-corrector algorithm that utilizes the CMFD adjoint flux to generate point kinetics parameters. A modified predictor-corrector quasi-static method is implemented in NECP-X [9], where a high-order polynomial function is employed to interpolate the kinetics parameters. On the other hand, PROTEUS-MOC [10] uses a finite-element-based MOC solver in the radial plane and a discontinuous Galerkin method-based 1D solver in the axial direction. However, the solution procedure used to solve the time-dependent neutron transport equation is identical. The time-dependent transport equation transforms into a steady-state equation called transient fixed source problem (TFSP).

This paper utilizes the 3D method of characteristics/diamond-difference (MOC/DD) [12] solution to generate cell surface current and CMFD correction factors. Finally, 3D pin-wise CMFD provides the overall solution. The transport code STREAM [13] applied the MOC/DD method to solve the MOC equation and implemented a pin-based pointwise energy slowing-down method [14,15] during the slowing-down calculation. The MOC/DD method accurately solves a problem where transport corrected [16] or anisotropic scattering [17] cross-sections are used. The 3D CMFD represents the whole-core transport problem and utilizes pin-cell homogenized cross-sections generated adaptively from the MOC/DD solution. The MOC calculation is performed to determine the core neutron fluxes at the flat source regions. The flux-volume weighting method generates the pin-cell homogenized cross-sections based on the local flat source region fluxes. The regional microscopic cross-sections are evaluated considering the local thermal condition. The cell cross-sections are fed into the 3D CMFD problem, which makes the global neutron balance. The CMFD solution provides the 3D flux and power distributions for the CMFD node structure. The 3D CMFD solver becomes the primary solver, while the MOC solver functions merely as the regional flux shape generator.

Moreover, the MOC solver has an additional function of generating the radial cell coupling coefficients, which relate to cell surface average current with two cell average fluxes. The cell CMFD correction factors and homogenized cross-sections are updated once the MOC calculation is completed. Any reactor condition changes, such as control rod movement, boron concentration change, or fuel temperature change, can reflect in the cell cross-sections and coupling coefficients. Hence, MOC recalculates regional microscopic cross-sections at the reactor's new thermal or operating conditions and performs flux-volume weighting.

In this paper, we used CMFD that represented the core overall power with pin-cell wise fluxes. In general, the predictor-corrector quasi-static methodology employs to generate overall power and fluxes. The MOC/DD method is used to generate the average cell surface current and diffusion coefficients ($\tilde{D}$). On the other hand, we incorporate two-level CMFD which is faster compare to typical CMFD. A two-level CMFD also use to accelerate the MOC solution.

2. Methodology

The derivation of the transient equation begins with the time-dependent multigroup CMFD equation. The time-dependent CMFD equation is then discretized using the theta method. The process of the transient fixed source problem solution is formulated in section 2.1. Later, the whole process with a flow diagram of the entire calculation is formulated in section 2.2.

2.1. Time dependent multigroup neutron diffusion equation

The time-dependent neutron balance equation for an energy group g, delayed neutron precursor group k, and computational node m is defined by:

$$\frac{1}{v_{g,m}}\frac{d\phi_{g,m}}{dt}=\chi_{pg}(1-\beta_m)S_{F,m}+\chi_{dg}S_{d,m}+\sum_{\substack{g'=1\\g'\neq g}}\Sigma_{gg',m}\phi_{g',m}-\left(\sum_{u=x,y,z}\frac{1}{h_{u,m}}\left(\sum_{u=x,y,z}\frac{1}{h_{u,m}}\left(J_{gu,m+}-J_{gu,m-}\right)\right)+\Sigma_{rg,m}\phi_{g,m}\right), \tag{1}$$

$$\frac{dC_{k,m}}{dt}=\beta_m S_{F,m}-\lambda_k C_{k,m}. \tag{2}$$

where $\phi_{g,m}$ and $C_{k,m}$ are the average neutron flux and average delayed neutron precursor density, and $S_{F,m}$ and $S_{d,m}$ are the total fission and delayed neutron source defined as,

$$S_{F,m}=\sum_{g=1}^{G}\nu\Sigma_{fg,m}\phi_{g,m} \tag{3}$$

$$S_{d,m}=\sum_{k=1}^{K}\lambda_k C_{k,m} \tag{4}$$

The average surface current along the direction u at the positive and negative side can be defined by CMFD relation,

$$J_{gu,m\pm}=\tilde{D}_{gu,m\pm}\left(\phi_{gu,m\pm}-\phi_{g,m}\right)-\hat{D}_{gu,m\pm}\left(\phi_{gu,m\pm}+\phi_{g,m}\right) \tag{5}$$

where $m\pm$ is the index of the neighbor node in positive and negative u directions, and $\tilde{D}_{gu,m\pm}$ and $\hat{D}_{gu,m\pm}$ are the corrective coupling coefficients. It is assumed that the corrective coupling coefficient $\tilde{D}_{gu,m\pm}$ is known from the MOC, and $\hat{D}_{gu,m\pm}$ is to be determined during the CMFD solution process.

The neutron diffusion equation for time step size Δt_n at time step n can be discretized using the theta method:

$$\frac{1}{v_{g,m}}\frac{\phi^n_{g,m}-\phi^{n-1}_{g,m}}{\Delta t_n}=\theta R^n_{g,m}+(1-\theta)R^{n-1}_{g,m}$$

$$\text{or},\frac{1}{\theta v_{g,m}}\frac{\phi^n_{g,m}-\phi^{n-1}_{g,m}}{\Delta t_n}=R^n_{g,m}+\left(\frac{1}{\theta}-1\right)R^{n-1}_{g,m} \tag{6}$$

where $R^n_{g,m}$ denoting all the right side of Equation (1) and

$$R^n_{g,m}=\chi_{pg}(1-\beta_m)S_{F,m}+\chi_{dg}S_{d,m}+\sum_{\substack{g'=1\\g'\neq g}}\Sigma_{gg',m}\phi_{g',m}-\sum_{u=x,y,z}\frac{1}{h_{u,m}}\left(\sum_{u=x,y,z}\frac{1}{h_{u,m}}\left(J_{gu,m+}-J_{gu,m-}\right)\right)+\Sigma_{rg,m}\phi_{g,m}\Bigg).$$

Moving the time-dependent term to the right side and rearranging the transient CMFD equation from Equation (6)

$$\sum_{u=x,y,z}\frac{1}{h_{u,m}}\left(J_{gu,m+}-J_{gu,m-}\right)+\Sigma_{rg,m}\phi_{g,m}=\chi_{pg}(1-\beta_m)S_{F,m}+\chi_{dg}S_{d,m}+\sum_{\substack{g'=1\\g'\neq g}}\Sigma_{gg',m}\phi_{g',m}-\frac{1}{\theta v_{g,m}}\frac{\phi^n_{g,m}-\phi^{n-1}_{g,m}}{\Delta t_n}+\left(\frac{1}{\theta}-1\right)R^{n-1}_{g,m}. \tag{7}$$

At the same time, the delayed neutron precursor term can be expressed from Equation (2)

$$\frac{dC_{k,m}e^{\lambda_k t}}{dt}=e^{\lambda_k t}\beta_m S_{F,m}. \tag{8}$$

The total fission source at time t can be expressed as a second-order expansion in terms of the total fission sources at time steps t_n, t_{n-1}, and t_{n-2}:

$$\beta_m S_{F,m}\approx\beta^n_m S^n_{f,m}\frac{\tilde{t}^2+\tilde{t}\gamma\Delta t_n}{(1+\gamma)(\Delta t_n)^2}+\beta^{n-1}_m S^{n-1}_{F,m}\left(1-\frac{\tilde{t}^2+(\gamma-1)\Delta t_n\tilde{t}}{\gamma(\Delta t_n)^2}\right)+\beta^{n-2}_m S^{n-2}_{F,m}\frac{\tilde{t}^2-\Delta t_n\tilde{t}}{(1+\gamma)\gamma(\Delta t_n)^2} \tag{9}$$

where $\tilde{t}=t-t_{n-1}$, and $\gamma=\frac{\Delta t_{n-1}}{\Delta t_n}$.

By integrating Equation (8) from the time t_{n-1} to t_n and substituting the term $\beta_m S_{F,m}$ with Equation (9), the precursor source can be expressed in any CMFD cell by:

$$C^n_k=\Omega^0_k(\tilde{\lambda}^n_k)C^{n-1}_k+\frac{1}{\lambda^n_k}\left(\beta^n_k S^n_F\Omega^n_k(\tilde{\lambda}^n_k)+\beta^{n-1}_k S^{n-1}_F\Omega^{n-1}_k(\tilde{\lambda}^n_k)+\beta^{n-2}_k S^{n-2}_F\Omega^{n-2}_k(\tilde{\lambda}^n_k)\right) \tag{10}$$

where

$$\tilde{\lambda}^n_k=\lambda^n_k\Delta t_n,$$

$$\Omega^0_k(\tilde{\lambda}^n_k)=E(\tilde{\lambda}^n_k)$$

$$\Omega^n_k(\tilde{\lambda}^n_k)=\frac{k_2(\tilde{\lambda}^n_k)+\gamma k_1(\tilde{\lambda}^n_k)}{(1+\gamma)}$$

$$\Omega^{n-1}_k(\tilde{\lambda}^n_k)=k_0(\tilde{\lambda}^n_k)-\frac{k_2(\tilde{\lambda}^n_k)+(\gamma-1)k_1(\tilde{\lambda}^n_k)}{\gamma}$$

$$\Omega^{n-2}_k(\tilde{\lambda}^n_k)=\frac{k_2(\tilde{\lambda}^n_k)-k_1(\tilde{\lambda}^n_k))}{(1+\gamma)\gamma},$$

$$\gamma=\frac{\Delta t_{n-1}}{\Delta t_n},E(x)=e^{-x}$$

$$k_0(x)=1-e^{-x},k_1(x)=1-\frac{k_0(x)}{x},k_2(x)=1-\frac{2k_1(x)}{x}$$

The delayed neutron precursor source can be expressed by:

$$S^n_{d,m}=\sum_{k=1}^{K}\lambda_k C^{n-1}_{k,m}e^{-\lambda_k\Delta t_n}+\sum_{l=n-2}^{n}\sum_{k=1}^{K}\beta^m_{k,m}\Omega^l_{k,m}S^l_{F,m}=\tilde{S}^{n-1}_{d,m}+\omega^{m,n}S_F \tag{11}$$

where

$$\omega^{m,n}=\sum_{k=1}^{K}\beta_{k,m}\Omega^n_{k,m}(\tilde{\lambda}^n_k)$$

$$\tilde{S}^{n-1}_{d,m}=\sum_{k=1}^{K}\lambda_k\Omega^0_{k,m}(\tilde{\lambda}^n_k)C^{n-1}_{k,m}+S^{n-1}_F\sum_{k=1}^{K}\beta^{n-1}_{k,m}\Omega^{n-1}_{k,m}(\tilde{\lambda}^n_k)+S^{n-2}_{F,m}\times\sum_{k=1}^{K}\beta^{n-1}_{k,m}\Omega^{n-2}_{k,m}(\tilde{\lambda}^n_k)$$

2.2. Solution of transient analysis

Multigroup CMFD problems defined by Equation (1) to Equation (11) are used to solve the TFSP, and the source iteration technique is used to solve the above equations. The convergence becomes slower if the number of energy groups increases or a massive perturbation occurs in the time step. The two-level CMFD scheme is introduced to resolve the above problem. The assembly-wise CMFD scheme serves as an acceleration scheme for the multigroup pin-wise CMFD problem. The effectiveness of the two-level scheme is excellent and reduces one-half time compared to single pin based CMFD. The MOC solution updates the cell average current and the coupling coefficient of the CMFD. So, the MOC solver recalls whenever a new change in the operating condition of the reactor occurs. A two-level CMFD is also incorporated into the MOC solver to make the solution faster.

The steady-state transport solver with TH feedback is used to get the forward flux of the problem at the initial state. The transport problem is condensed to the pin level and generates cell cross-sections, and the flux-volume weighting method is used to update the cell cross-sections. CMFD adjoint fluxes are computed after getting steady-state cell cross-sections and CMFD correction factors. The delayed neutron sources and precursor concentrations are initialized using the forward CMFD flux. CMFD flux represents the core power, and the MOC solver accelerated by a two-level CMFD is used only for updating CMFD cell cross-sections and correction factors. So, the MOC solver will call when cell cross-sections and CMFD correction factors ($\tilde{D}$ and $\hat{D}$) change. On the other hand, TH updates and adjustments of the transport solution are made every time step because the transport solution has a delayed neutron equation. The MOC solution will be inaccurate if the delayed neutron precursors concentrations are calculated improperly. A complete flow chart of the TFSP structure is shown in Fig. 1 and the scheme details as follows:

1. Perform the steady-state calculation with the CMFD adjoint calculation.
2. Cross-section perturbed > δ
   a. Perform the transport calculation with a time step Δt to achieve the average current and scalar flux.
   b. Update the CMFD correction factors (coupling coefficients) using Equation (5).
3. Performed the CMFD calculation using Equation (7).
4. Adjust transport solution.

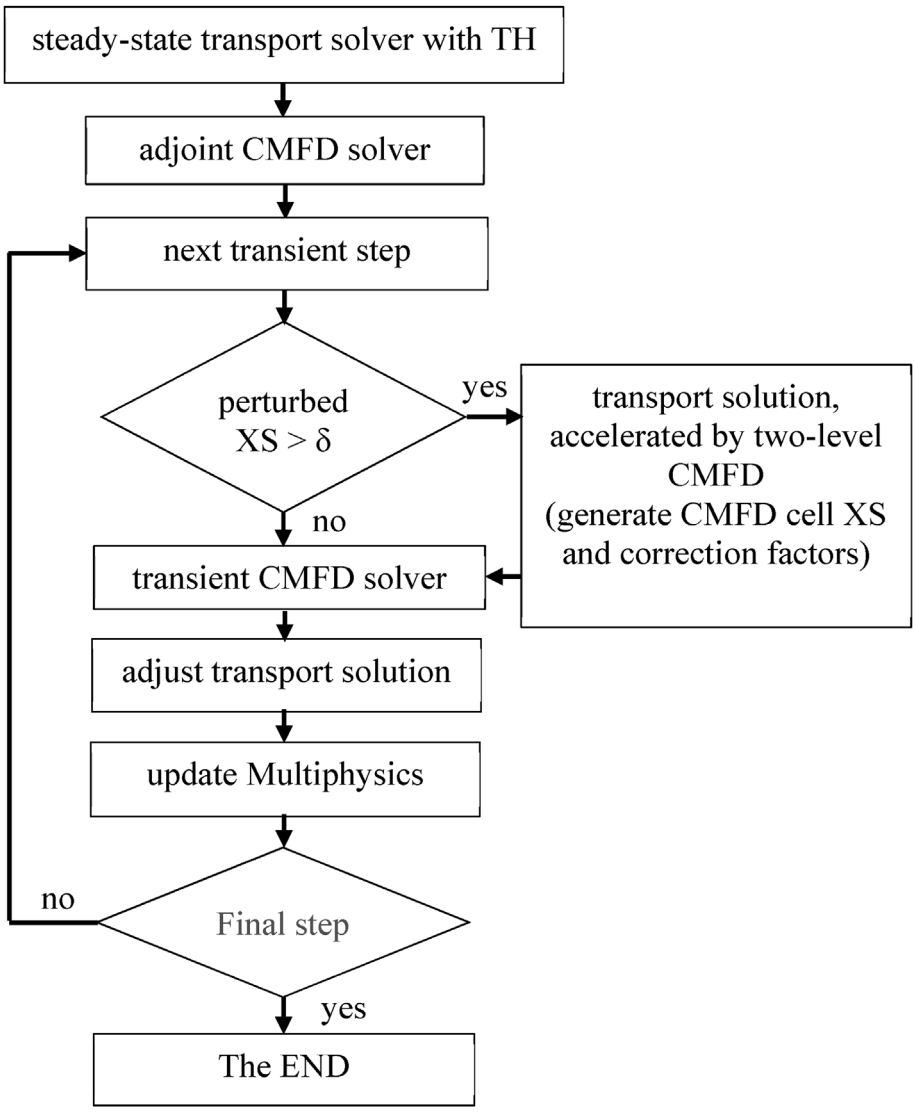

Fig. 1. Flow diagram of CMFD based transient fixed source problem.

5. Update Multiphysics (optional).
6. Update delayed neutron precursor density using Equation (11).
7. Repeat steps 2–6 until the final time step.

3. Rod decusping technique

The reactor core configuration dynamically changes due to the control rod's movement in the regular reactor operation. When a control rod is partially inserted into a cell, a new material identification is needed. A partially rodded node is present whenever the control rod tip location does not precisely match the axial nodal interface. One way to resolve this problem is using the moving meshes technique, where the spatial mesh is moved together with the control rods so that there are no partially inserted cells [18]. A high-order polynomial is employed to interpolate the old mesh solution to the following mesh solution.

A partially rodded node is explored in Fig. 2, where a proper treatment of the axially homogenized cross sections is necessary to alleviate the control rod decusping effect. Correcting the cell cross-sections is simply utilizing weighted average cell values. The flux represented in a partially rodded node k with height h_k can be approximated into rodded (R) and unrodded (U) average flux. This strategy is known as the approximate flux weighting method [19,20]. The rodded and unrodded average flux in a partially rodded node k is,

$$\phi_k^R = \frac{f_{in} h_k \phi_k + h_{k+1} \phi_{k+1}}{f_{in} h_k + h_{k+1}} \tag{12}$$

$$\phi_k^U = \frac{(1 - f_{in}) h_k \phi_k + h_{k-1} \phi_{k-1}}{(1 - f_{in}) h_k + h_{k-1}} \tag{13}$$

where h and ϕ represent the respective node's axial height and average flux.

The homogenized cross-sections in the partially rodded node k can be updated as follows:

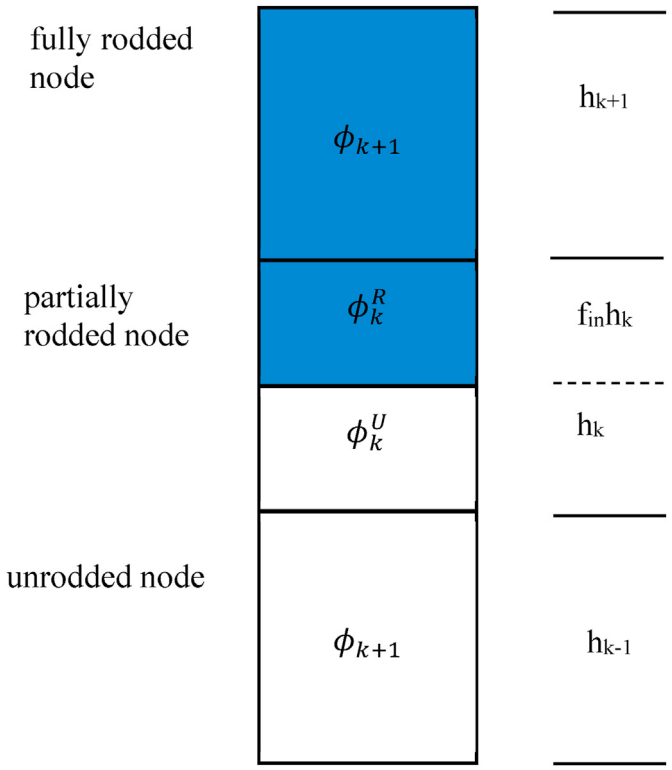

Fig. 2. Rod decusping in partially rodded node.

$$\Sigma_k^{eff} = \frac{\Sigma_k^R f_{in}\phi_k^R + \Sigma_k^U(1-f_{in})\phi_k^U}{f_{in}\phi_k^R + (1-f_{in})\phi_k^U} \tag{14}$$

where Σ_k^R and Σ_k^U represent the cross-sections of the rodded and unrodded part of the cell, respectively, and ϕ_k^R and ϕ_k^U represent the average flux of the rodded and unrodded part of the cell, respectively.

4. Adaptive time-step control

The computational cost is the most valuable issue for transient analysis. A small-time step may ensure good solution approximations and increase the computational cost. On the other hand, the computational cost is minor by using giant time steps, which may generate inaccurate results. Moreover, shorter time steps may not be necessary for some transient stages. Implementation of adaptive control of the time step is the way to overcome this difficulty. The local truncation error at any given step is proportional to the step size, and the error represents by,

$$\varepsilon = C\Delta t^{p+1}, \tag{15}$$

where the coefficient vector C is O(1) as $\Delta t \to 0$.

The step size for the next step, Δt_{n+1}, is chosen as [21]

$$\Delta t_{n+1} = \gamma \Delta t_n \left(\frac{tol.\Delta t_n}{|\varepsilon|}\right)^{1/p}, \tag{16}$$

where γ is a safety factor chosen ≤ 1. A typical choice is $\gamma = 0.9$, and the tolerance value tol > 0, p is a method of order, and choice p = 2. The calculated step is rejected and recalculated when the error $|\varepsilon|$ is massive ($|\varepsilon| > Q.tol.\Delta t_n$). A typical value of Q is 1.2.

The local errors are estimated depending on the variation in the cross-sections or neutron flux changes. The perturbed cross-sections error is,

$$\varepsilon_{xs}^n = \sum_{g,m} \frac{\left|\left(XS_{g,m}^n - XS_{g,m}^{n-1}\right)\right|}{\left|XS_{g,m}^{n-1}\right|} \tag{17}$$

where g and m are the energy group and the cell index, respectively.

Another approach is to calculate the maximum neutronic flux error at time step n, which can be defined by:

$$\varepsilon_{md}^n = \max_m \frac{\left|\left(\phi_{g,m}^n - \phi_{g,m}^{n-1}\right)\right|}{\left|\phi_{g,m}^{n-1}\right|}. \tag{18}$$

A logical equation can be applied to select the error, which is used to update the time step as follow:

$$|\varepsilon| = \varepsilon_{xs}^n \text{ or } \left(\text{not}(\varepsilon_{xs}^n) \text{ and } \varepsilon_{md}^n\right). \tag{19}$$

In a word, Equation (17) will be valid only when the reactor's control rod movement or thermal change occurs, or Equation (18) will always be true except for control rod movement and thermal changes.

The time step size for the time step (n+1) can be defined by Ref. [22]:

$$\Delta t_{n+1} = \Delta t_n \left[\min\left(2.0, \max\left(0.5, \gamma\left(\frac{tol.\Delta t_n}{|\varepsilon|}\right)^{1/p}\right)\right)\right] \tag{20}$$

where the unit of the time is second.

5. Numerical results

The numerical results section contains three problems: (1) a mini-core 3D problem to check the performance of parallel computing and adaptive time step control, (2) the 3D heterogeneous C5G7-TD benchmark to verify the relative error and control rod decusping effect, and (3) a practical whole-core problem to show the performance of CMFD for the rod-ejection transient.

5.1. 3D mini-core problem

The mini-core problem consists of nine assemblies with 3 × 3 configurations. The reflective boundary condition was used on all the radial sides, and the quarter core model is considered for analysis because of symmetry. The complete radial and axial arrangement of the core geometry of the problem is shown in Fig. 3. The assembly size was similar to an ordinary conventional assembly, and the length of the assembly pitch was 21.42 cm. The axial core height was the same as the traditional assembly of reactor height. The core consists of a 21.42 cm top and bottom reflector, and an identical homogenized cross-section was used for the reflector. The control rod of the assembly is not inserted on the top side of the reflector. The height of the active core was 365.76 cm, and two groups of homogenized cross-sections and six groups of delayed neutron precursors are given in Ref. [23]. The feedback effect due to the thermal-hydraulic (TH) change is not considered in the problem.

Four types of cross-section data were used. UOX, UOXR, UOXF, and MOX indicate un-rodded, rodded, fresh uranium oxide fuel (UOX) and mix-oxide fuel homogenize cross-sections, respectively. In the axial top half (182.88 cm) of the assembly, UOXR (Fig. 3 radial

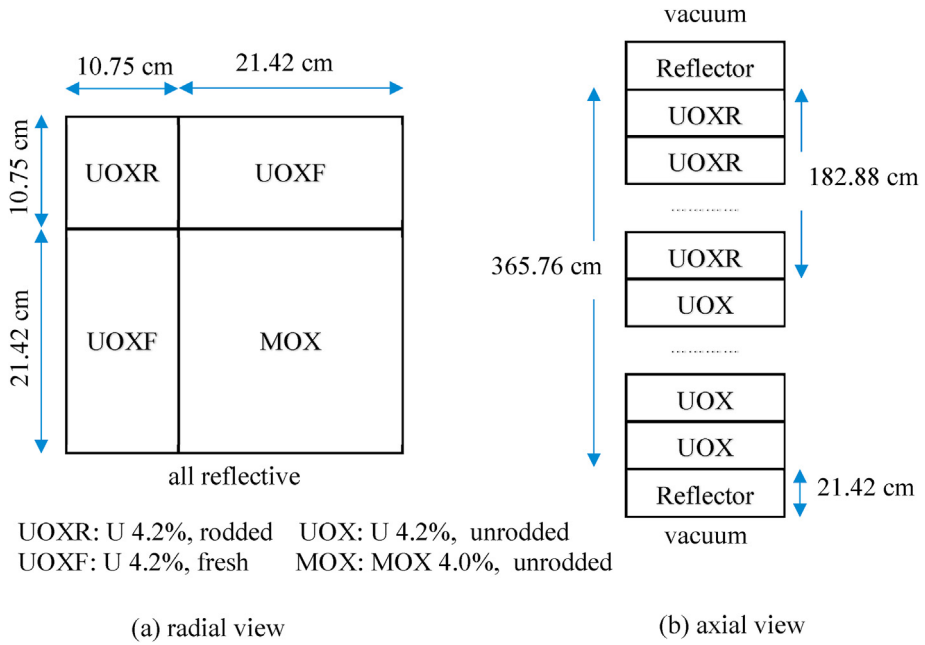

Fig. 3. Configuration for the mini-core problem, (a) radial view and (b) axial view.

Table 1
k-effective and ejected rod worth for the mini-core 3D problem.

Codes	All rod out (ARO)		All rod in (ARI)		Ejection rod worth ($)
	k-effective	error (pcm)	k-effective	error (pcm)	
DeCART	1.08660	–	1.08019	–	0.719
STREAM	1.08662	2	1.08024	5	0.715

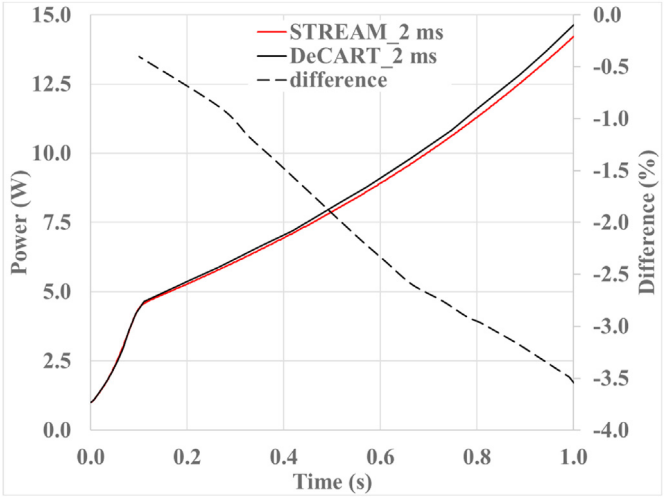

Fig. 4. Power history of the mini-core problem.

view) cross-section was perturbed within 0.1 s. The perturbation procedure moves linearly from bottom to top. During perturbation, the UOXR cross-section set was replaced with the UOX cross-section, and there would be no more UOXR cross-section in the assembly after 0.1 s.

A steady-state analysis of the rodded and unrodded conditions of the problem is shown in Table 1. It is clear from the table that the effective multiplication factor and ejected rod worth are close to the reference results. The maximum difference of k-effective was 5 pcm. The relative power history with DeCART is shown in Fig. 4, and a comparison study of the normalized assembly power is shown in Table 2. The parallelization and adaptive time step control performance are shown in Table 3. A total of 17.65 h is required for a 1-s

Table 2
Assembly power comparisons for the Mini-core 3D problem.

Time (s)	Position	STREAM		Time (s)	Position	STREAM	
		Power	Diff. %			Power	Diff. %
0.0	UOXR	0.9126	0.07	0.2	UOXR	0.9743	−0.07
	UOXF	1.0280	0.00		UOXF	1.0260	−0.10
	MOX	0.9942	0.03		MOX	0.9799	−0.01
0.4	UOXR	0.9743	−0.07	0.6	UOXR	0.9743	−0.07
	UOXF	1.0260	−0.10		UOXF	1.0260	−0.10
	MOX	0.9799	−0.01		MOX	0.9799	−0.01
0.6	UOXR	0.9743	−0.07	1.0	UOXR	0.9743	−0.07
	UOXF	1.0260	−0.10		UOXF	1.0260	−0.10
	MOX	0.9799	−0.01		MOX	0.9799	−0.01

Table 3
Performance of parallelization and adaptive time step control.

Technique	Process/thread	Step size (ms)	Time
–	1	2	17.65 h.
OPENMP	9	2	1.85 h.
OPENMP	9	Adaptive control	55.90 min
MPI	9	2	1.36 h.
MPI	9	Adaptive control	40.42 min

Table 4
Performance of two-level CMFD (accelerate MOC).

Step (ms)	Process/thread	Standard CMFD	Two-level CMFD	Time reduction
2	9	242 min	110 min	0.45
5		140 min	56 min	0.40
10		80 min	31 min	0.39
20		58 min	20 min	0.34
50		37 min	15 min	0.41

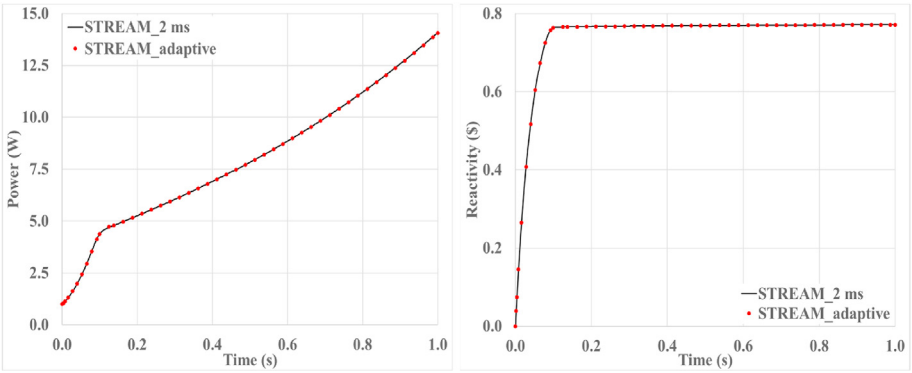

Fig. 5. Power and reactivity history of STREAM for the mini-core problem.

simulation (2 ms step size) using a single CPU. On the other hand, computational time reduces to less than 2 h using nine processes/threads. Implementation of adaptive time step control reduces it to less than 1 h by utilizing the same number of processes/threads. The performance of CMFD acceleration is shown in Table 4. The relative power and reactivity accuracy with fixed and adaptive time steps are shown in Fig. 5.

5.2. C5G7-TD benchmark problem

A minuscule light water reactor (LWR) benchmark is C5G7-TD [20], which has sixteen fuel assemblies (eight uranium oxides (UO_2) fuels and eight mixed oxide (MOX) fuels) surrounded by a water reflector. The lattice size of the assembly is a 17 × 17 array with 364 fuel pins, 24 guide tubes, and one instrument tube in the

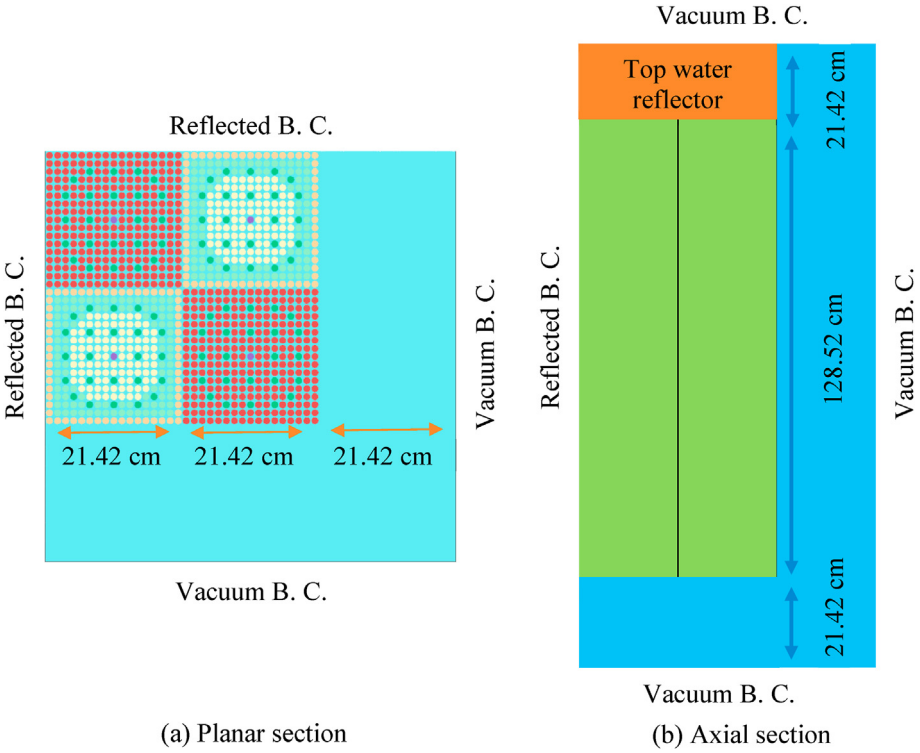

Fig. 6. 3D configuration of the C5G7-TD problem.

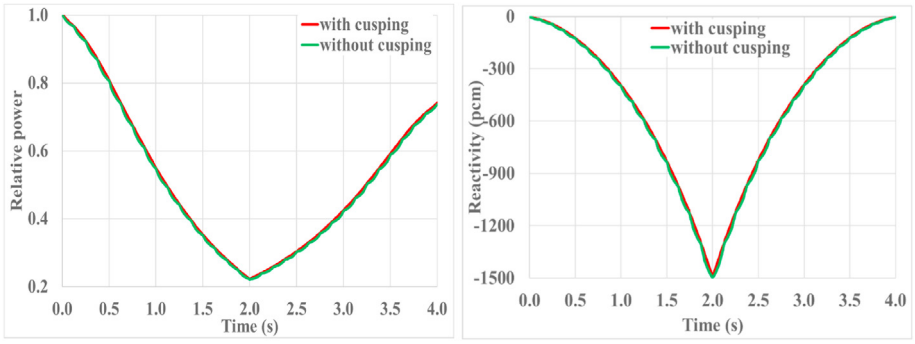

(a) Fractional fission rate history (b) Reactivity history

Fig. 7. Control rod decusping effect on the core power and reactivity (C5G7-TD4-1).

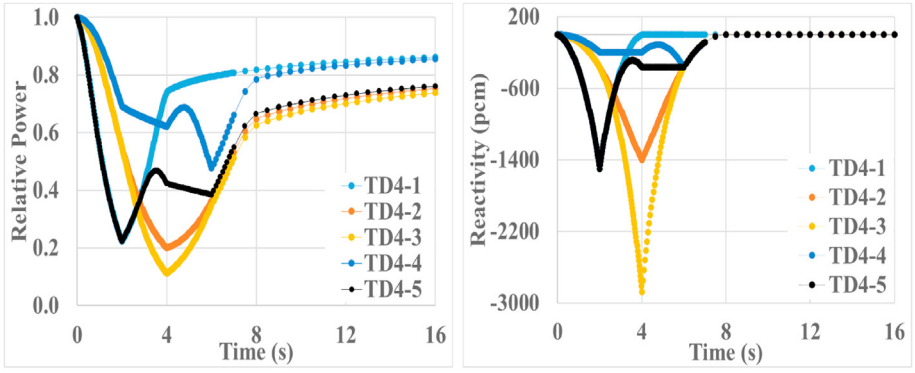

(a) Fractional fission rate history (b) Reactivity history

Fig. 8. Results for exercise C5G7-TD4.

center grid cell. This problem does not utilize spatial homogenization above the fuel pin level, and three enrichments of 4.3%, 7.0%, and 8.7% fuels are used in the MOX assembly. All pin cells have a pin radius of 0.54 cm, and the assembly and pin pitches were 21.42 cm and 1.26 cm, respectively. Each pin geometry has an inner and outer region. The outer part corresponds to the moderator, and the internal zone indicates a mixture of all objects (fuel, gap, and clad). Fuel, guide tube, fission chamber, moderator, and control rod materials have individual seven-group transport corrected macroscopic cross-sections. The benchmark was initially designed for a 2D problem, but minor modification is adopted in the axial direction to make the 3D geometry, as shown in Fig. 6. The axial height of the active core is 128.52 cm, excluding 21.42 cm lower and upper axial reflectors. Control rods of the problem are permanently implanted into the upper reflector, and TH feedback change is not considered in the benchmark.

Table 5
Relative errors (%) of the core power history from different codes to STREAM results (16 s transient).

	MPACT			nTRACER PSI			RMC		
	RMS	MAX	Avg.	RMS	MAX	Avg.	RMS	MAX	Avg.
TD4-1	0.26	−1.55	0.20	0.98	4.28	0.82	0.47	−2.10	0.41
TD4-2	0.45	3.11	0.36	0.26	1.47	0.20	1.08	4.89	0.90
TD4-3	0.49	3.52	0.37	0.33	3.48	0.27	1.56	−19.93	1.37
TD4-4	0.31	1.50	0.25	0.28	1.48	0.24	1.26	−4.09	1.03
TD4-5	0.97	3.33	0.90	0.77	5.52	0.53	1.84	−14.14	1.61

In 3D configuration, the insertion and withdrawal of the control rod are analyzed. The core control rod bank was un-rodded at the initial condition of each problem, and the rod bank moved at a constant speed. It is assumed that a total of 6 s is required to insert or withdraw the rod bank from the active core's bottom position to the active core's top position. The C5G7-TD4 exercise has five sub-problems:

- TD4-1: bank 1 insertion/withdrawal.
- TD4-2: bank 3 insertion/withdrawal.
- TD4-3: bank 1 and 3 insertion/withdrawal.
- TD4-4: bank 3 and 4 insertion/withdrawal.
- TD4-5: bank 1 and 3 insertion/withdrawal.

The benchmark exercise TD4-1 was chosen to check the control rod decusping effect. In this test, control rod bank one moved at a constant speed to a maximum depth of 33% of the active core height, and the bank moved again to the original position. The relative power and reactivity of TD4-1 are shown in Fig. 7. The cyan color curve was obtained without any decusping treatment. In contrast, the red color curve was obtained with the decusping treatment described in section 4. The power and reactivity obtained without treatment are polluted by decusping effects.

The relative power and reactivity history of TD4 in all exercises are shown in Fig. 8. A fixed time step (25 ms) is used throughout the 16 s transient. Table 5 shows the relative core power errors in percent, and the reference results are taken from Ref. [24]. The results of the STREAM compared with those of MPACT, nTRACER

from PSI, and RMC. The relative error versus time is shown in Fig. 9. The STREAM results show excellent agreement with the code results from MPACT and nTRACER. The differences in outcomes between STREAM and other deterministic codes are smaller than those between STREAM and the Monte Carlo code RMC. Oscillation in the relative errors was observed during the control rod insertion and withdrawal stage due to the decusping methods used by different codes. The maximum amplitude of the relative error was 3.52% for exercise TD4-3 compared to MPACT. The relative errors were much smaller in the deterministic code when the control rod was not moving. However, less than 1% RMS and relative average error were observed for all exercises, and the maximum RMS and relative average error were noted at 0.97% and 0.90%, respectively, for the exercises TD4-5. It is noted that 14 CPU cores (Intel Xeon Gold 5222 3.80 GHz) are used to perform the calculations, and the summary time is tabulated in Table 6.

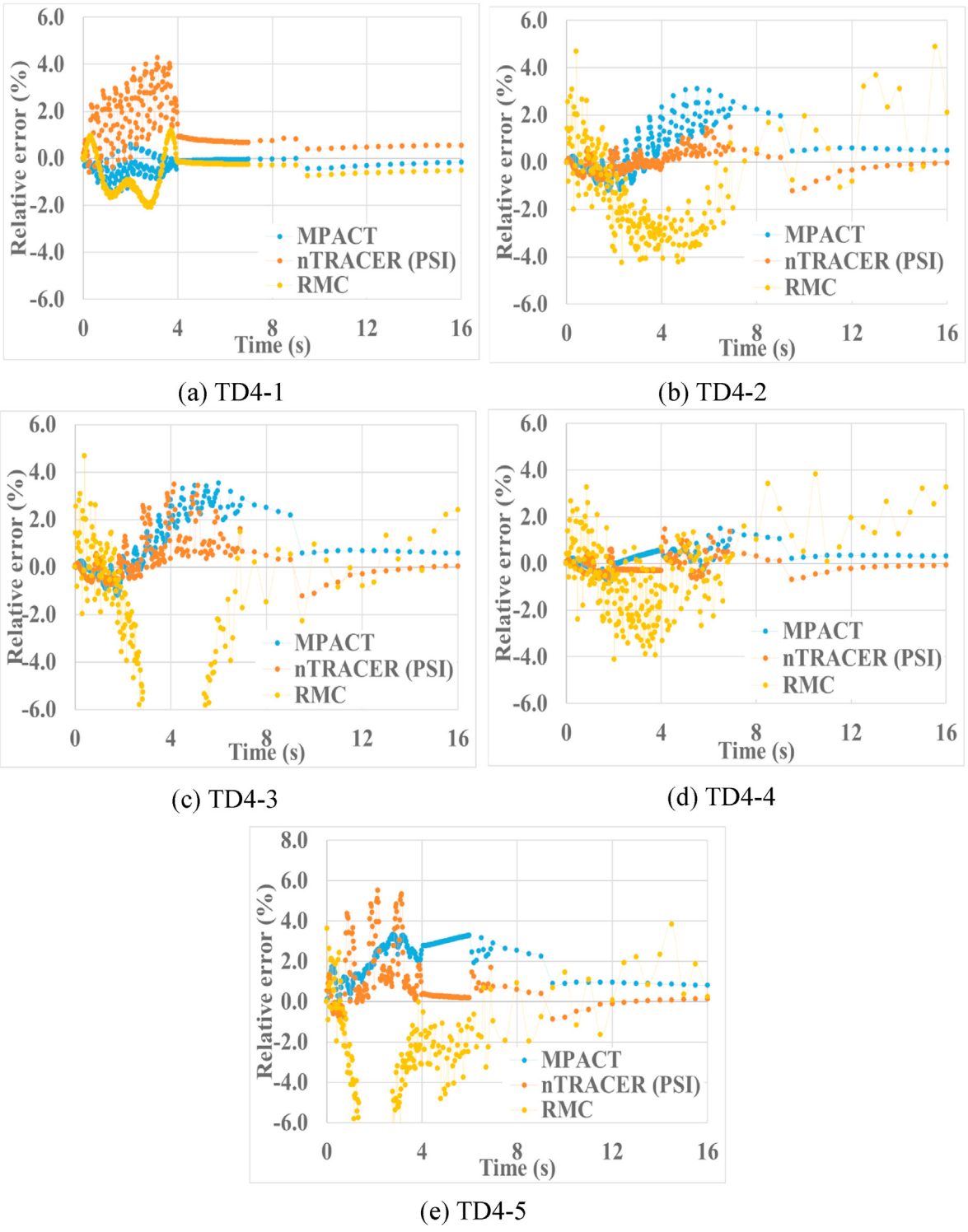

Fig. 9. Relative errors of the C5G7-TD4 fractional core fission rates from different codes to STREAM results.

Table 6
Run time summary for the C5G7-TD4 problem (16 s transient).

Case	1	2	3	4	5
TD4	22.28 h	34.56 h	38.16 h	24.24 h	31.44 h

5.3. Whole-core problem

A typical reactor core, OPR1000, was selected to test the performance of the code with TH feedback. A complete loading pattern of the cycle 1 core is shown in Fig. 10(a), and the core is composed of 177 fuel assemblies with a 16 × 16 array of 236 fuel pins and five guide tubes. The test was performed at hot zero power conditions, and technical information about the core is shown in Table 7. The total thermal power of the core is 2815 MWth with a coolant flow of 16315.0 kg/s and 569.25K inlet temperature. Three different enrichments of fuel (A, B, and C) were used, varying from 1.42 wt% to 3.42 wt%. The control rod configuration of the core is shown in Fig. 10(b), and it includes regulating bank (R1-R5), shutdown bank (SA, SB), and part strength (PS). The beginning of the cycle core was selected because the total enthalpy of the core at the beginning of the cycle is higher under rod ejection accident (REA) compared to the end of the cycle with a given prompt reactivity insertion [25]. The control rod bank R4 of the fresh fuel assembly was withdrawn in 0.1 s. The transport code, STREAM, was used to calculate a total 0.5 s transient simulation of the core neutronic and TH behavior during and after the control rod withdrawal. The withdrawal rate of the control rod was constant. A simple 1.5D code, TH1D, was used to calculate the coolant and fuel temperature of the core. It used a user-defined heat transfer coefficient (1.0×10^4 W/m^2.K). It is noted that 75 CPU cores (Intel Xeon Gold 5222 3.80 GHz) are used to perform the whole-core calculations, and 257.28 h (10.72 days) is required to complete a 0.5 s simulation.

The relative core power and reactivity history of the single rod bank (R4) REA accident is shown in Fig. 11. The number of time steps used to update the core power by using the MOC or without MOC are indicated on the reactivity plot. Black and red circles are identified as time steps using with and without MOC update, respectively. However, the results are not compared to those generated by other transport codes because of unavailability. A total of 1.20 $ reactivity was inserted when the control rod bank, R4, was entirely removed from the core. It is noted that a maximum of 802% core relative power was observed at 0.364 s, and inserted reactivity decreased from 1.20$ to 0.98 $ at that time.

Table 7
Technical information of OPR1000 core.

Description	Parameters
Type	Pressurized Water Reactor
Number of fuel assemblies	177
Assembly fuel matrix	16 × 16
Assembly size	21.42 × 21.42 cm
Core power	2815 MWth
Coolant flow	16315.0 kg/s
Inlet temperature	568.25 K
Transient initial power	10^{-4}% of core power (2815 MWth)
Control rod position	All regulating banks in and shutdown banks out
Eject control rod	R4
Ejection time	100 ms

A maximum of 22582 MWth core power was noted at 0.364 s, which indicates a core power increase of 8.02 times compared to normal reactor power. The fuel and coolant average temperatures increased to 612.12K and 569.44K, respectively. Finding an exact solution is difficult due to the unavailability of the reference results, but the current results indicate the code's capability with TH feedback. A maximum of 419 kW/m linear power and 881 MW s of released energy were observed at the peak power. A summary of peak point results is shown in Table 8. The core fuel and coolant average temperature is shown in Fig. 12 and core maximum linear power and energy released are shown in Fig. 13.

Table 8
Summary results at peak power.

Description	Parameters
Inserted reactivity (total)	1.20 $
Compensated reactivity at peak power	0.22 $
Core peak power	22582 MWth
Time to peak power	0.364 s
Relative peak power	8.02
Fuel average temperature	612.12 K
Coolant average temperature	569.44 K
Maximum fuel temperature	673.87 K
Maximum linear power rate	419 kW/m
Released energy	881 MW s

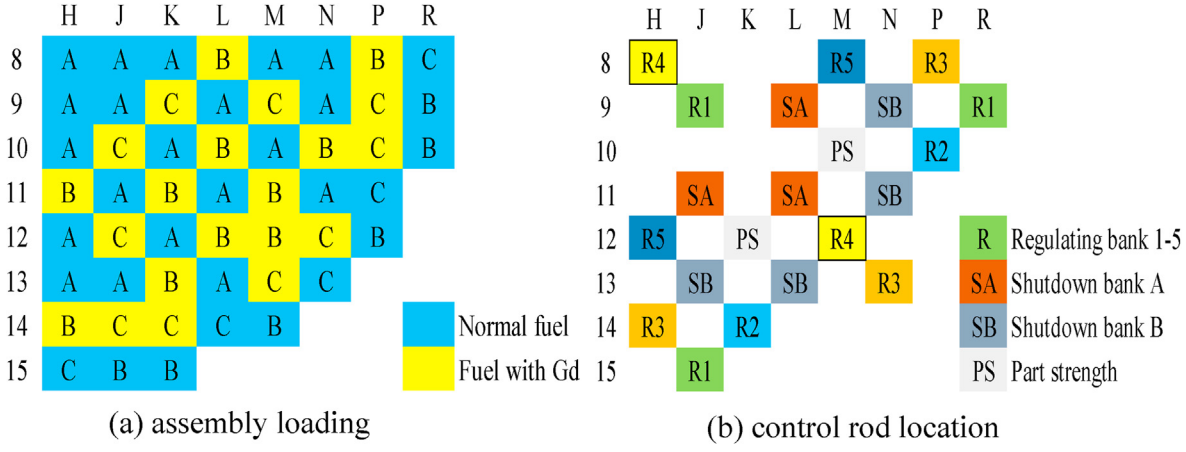

Fig. 10. Core configuration of the OPR1000.

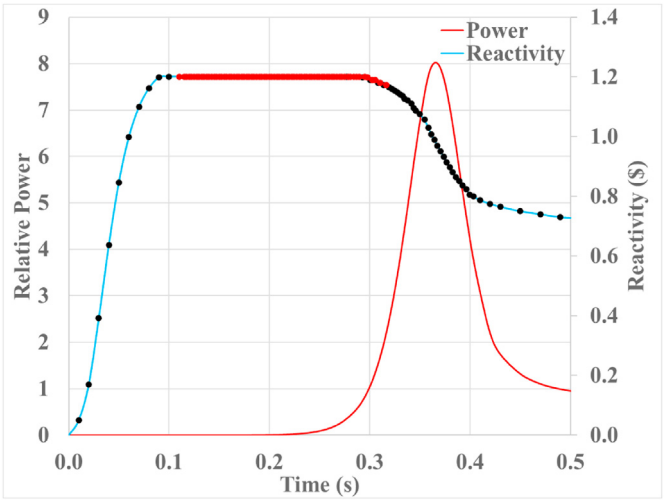

Fig. 11. Core relative power and reactivity history of the OPR1000.

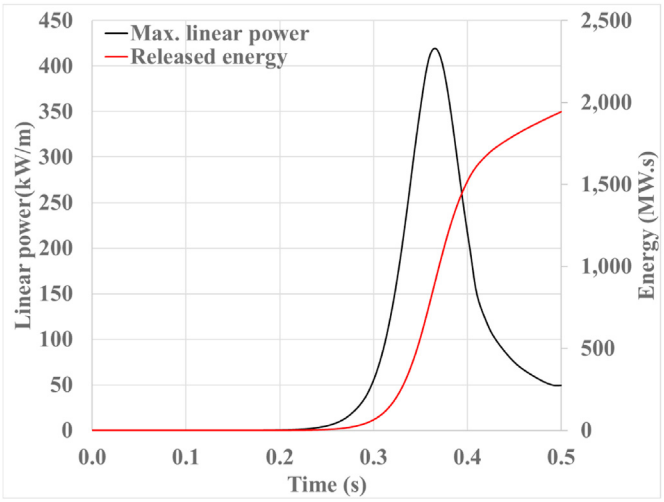

Fig. 13. Maximum linear power and energy released behavior of the OPR1000.

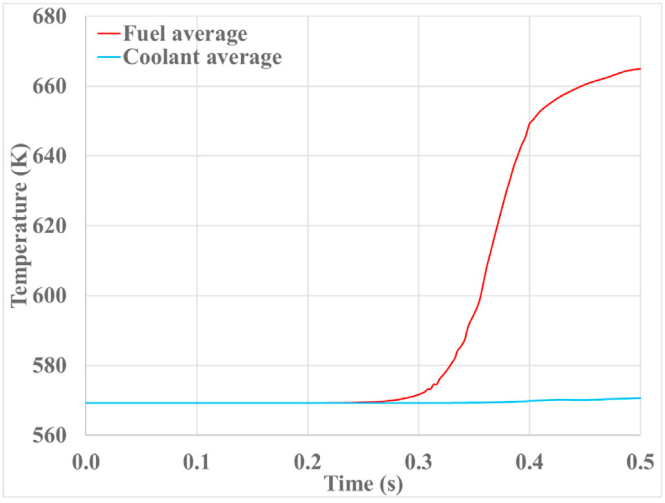

Fig. 12. Core average temperature behavior of the OPR1000.

6. Conclusions

The principal goal of this research was to develop algorithms to solve time-dependent neutron transport equations with pin-resolved detail for whole-core LWR applications. The transport equations are solved when the reactor condition changes, such as control rod movement, boron concentration change, or fuel temperature change, which can reflect in the cell cross-sections and CMFD correction factor (coupling coefficients). On the other hand, the transient CMFD equations are solved at each step to update the core flux. The numerical results show the accuracy of the developed scheme. The scheme was also designed with thermal-hydraulics feedback to work within the framework.

The various transient benchmarks were simulated with STREAM to verify the code's capability. 3D exercises contain several subgroups involving the insertion and withdrawal of control rods. The STREAM results have good agreement with those from other deterministic codes. The performance of time step control and parallel computing were studied, demonstrating the effectiveness of the method used in STREAM. It reduced computing costs without sacrificing the solution's accuracy. The REA accident scenario confirmed the ability of the transport code STREAM. In the REA accident case, a maximum of 802% reactor power was observed with 0.22 $ reactivity compensation at peak power. Hence, the transport code STREAM can simulate the transient behavior of the reactor core with TH feedback.

Declaration of competing interest

The authors declare that they have no known competing financial interests or personal relationships that could have appeared to influence the work reported in this paper.

Acknowledgement

This work was partially supported by a National Research Foundation of Korea (NRF) grant funded by the Korean government (MSIT) (No. NRF-2019M2D2A1A03058371) and the project (L20S089000) by Korea Hydro and Nuclear Power Co. Ltd. This work was partially supported by Korea Institute of Energy Technology Evaluation and Planning (KETEP) grant funded by the Korea government (MOTIE) [RS-2023-00241302]. The authors would like to express their sincere gratitude to Brendan Kochunas, Assistant Professor, Department of Nuclear Engineering and Radiological Sciences, University of Michigan, and Qicang Shen, Post-doctoral Researcher, the University of Michigan, for providing the MPACT results.

References

[1] M.A. Smith, E.E. Lewis, B.-C. Na, Benchmark on deterministic 2-D MOX fuel assembly transport calculations without spatial homogenization, Prog. Nucl. Energy 45 (2–4) (2004) 107–118, https://doi.org/10.1016/j.pnueene.2004.09.003.
[2] J.E. Hoogenboom, W.R. Martin, B. Petrovic, Monte Carlo performance benchmark for detailed power density calculation in a full-size reactor core, Benchmark specifications (2010) revision 1.2 July 2011, p3.
[3] K.S. Smith, J. Rhodes, CASMO characteristics method for two-dimensional PWR and BWR core calculation, Trans. Am. Nucl. Soc. 83 (2000) 294–296.
[4] S. H, The free lunch is over: a fundamental turn toward concurrency in software, Dr. Dobb's J. 30 (3) (2005).
[5] A. Rineiski, J.Y. Doriath, Time-dependent neutron transport with variational nodal method, Proc. Joint Int. Conf. on Math. Methods and Supercomputing for Nuclear Application (1997) 1661.
[6] J.-Y. Cho, K.-S. Kim, C.C. Lee, H.-G. Joo, W.-S. Yang, T.A. Taiwo, J. Thomas, Transient capability for a MOC-based whole core transport code DeCART, Trans. Am. Nucl. Soc. 92 (2005) 721–722.
[7] P.W. David, S. Tanju, W.S. Yang, J.D. Thomas, J.W. Thomas, Z. Zhong, J.Y. Cho, S.K. Kim, T.H. Chun, H.G. Joo, C.H. Kim, High-fidelity light water reactor analysis with the numerical nuclear reactor, Nucl. Sci. Eng. 155 (3) (2007)

395–408, https://doi.org/10.13182/NSE07-A2672.
[8] A. Zhu, Y. Xu, A. Graham, M.I. Young, T. Downar, L. Cao, Transient methods for pin-resolved whole core transport using the 2D-1D methodology in MPACT, in: M&C, 2015.
[9] B. Wang, Z. Liu, J. Chen, C. Zhao, L. Cao, H. Wu, A modified predictor-corrector quasi-static method in NECP-X for reactor transient analysis based on the 2D/1D transport method, Prog. Nucl. Energy 108 (2018) 122–135, https://doi.org/10.1016/j.pnucene.2018.05.014.
[10] T.N. Nguyen, Y.S. Jung, T. Downar, C. Lee, Implementation of the transient fixed-source problem in the neutron transport code PROTEUS-MOC, Ann. Nucl. Energy 129 (2019) 199–206, https://doi.org/10.1016/j.anucene.2019.01.005.
[11] N.Z. Cho, G.S. Lee, C.J. Park, Fusion of method of characteristics and nodal method for 3-d whole-core transport calculation, Trans. Am. Nucl. Soc. 86 (2002) 322–324.
[12] S. Choi, D. Lee, Three-dimensional method of characteristics/diamond-difference transport analysis method in STREAM for whole-core neutron transport calculation, Comput. Phys. Commun. 260 (2021), 107332, https://doi.org/10.1016/j.cpc.2020.107332.
[13] S. Choi, W. Kim, J. Choe, W. Lee, H. Kim, B. Ebiwonjumi, E. Jeong, K. Kim, D. Yun, H. Lee, D. Lee, Development of high-fidelity neutron transport code STREAM, Comput. Phys. Commun. 264 (2021), 107915, https://doi.org/10.1016/j.cpc.2021.107915.
[14] S. Choi, W. Kim, D. Lee, Refinements of pin-based pointwise energy slowing-down method for resonance self-shielding calculation-I: theory, Front. Energy Res. 20 (9) (2021), https://doi.org/10.3389/fenrg.2021.765863.
[15] W. Kim, S. Choi, D. Lee, Refinements of pin-based pointwise energy slowing-down method for resonance self-shielding calculation-II: verifications, Front. Energy Res. 15 (9) (2021), https://doi.org/10.3389/fenrg.2021.765865.
[16] S. Choi, K. Smith, H.C. Leec, D. Lee, Impact of inflow transport approximation on light water reactor analysis, J. Comput. Phys. 299 (15) (2015) 352–373, https://doi.org/10.1016/j.jcp.2015.07.005.
[17] A. Rahman, D. Lee, Incorporation of anisotropic scattering into the method of characteristics, Nucl. Eng. Technol. 54 (9) (2022) 3478–3487, https://doi.org/10.1016/j.net.2022.03.041.
[18] A. Vidal-Ferrandiz, R. Fayez, D. Ginestar, G. Verdú, Moving meshes to solve the time-dependent neutron diffusion equation in hexagonal geometry, J. Comput. Appl. Math. 291 (2016) 197–208, https://doi.org/10.1016/j.cam.2015.03.040.
[19] J.H. S, Resolution of the Control Rod Cusping Problem for Nodal Methods, Ph.D. Thesis, Dept. of Nuclear Engineering, Massachusetts Institute of Technology, 1984.
[20] V.F. Boyarinov, P.A. Fomichenko, J. Hou, M. Avramova, K. Ivanov, A. Aures, W. Zwermann, K. Velkov, H.G. Joo, Deterministic Time-dependent Neutron Transport Benchmark without Spatial Homogenization (C5G7-TD) Volume II: Dynamics Phase, OECD Nuclear Energy Agency, 2021.
[21] K. Gustafsson, M. Lundh, G. Derlind, A PI stepsize control for the numerical solution of ordinary differential equations, BIT Numerical Mathematics 28 (2) (1988) 270–287, https://doi.org/10.1007/BF01934091.
[22] A. Carreno, A. Vidal-Ferrandiz, D. Ginestar, G. Verdu, Adaptive time-step control for modal methods to integrate the neutron diffusion equation, Nucl. Eng. Technol. 53 (2) (2021) 399–413, https://doi.org/10.1016/j.net.2020.07.004.
[23] B. Cho, N.Z. Cho, A nonoverlapping local/global iterative method with 2-D/1-D fusion transport kernel and p-CMFD wrapper for transient reactor analysis, Ann. Nucl. Energy 85 (2015) 937–957, https://doi.org/10.1016/j.anucene.2015.07.012.
[24] Q. Shen, Y. Wang, D. Jabaay, B. Kochunas, T. Downar, Transient analysis of C5G7-TD benchmark with MPACT, Ann. Nucl. Energy 125 (2019) 107–120, https://doi.org/10.1016/j.anucene.2018.10.049.
[25] D.J. Diamond, B.P. Bromley, A.L. Aronson, Studies of the Rod Ejection Accident in a PWR, Brookhaven National Laboratory, 2002. W-6382 1/22/02.